ORIGINAL PAPER

Homoclinic bifurcation in a quasiperiodically excited impact inverted pendulum

Junming Gao · Zhengdong Du

Abstract Homoclinic bifurcation for a nonlinear inverted pendulum impacting between two rigid walls under external quasiperiodic excitation is analyzed. The results for the homoclinic bifurcation of quasiperiodically excited smooth systems obtained by Ide and Wiggins are extended to the non-smooth ones. We present a method of Melnikov type to derive sufficient conditions under which the perturbed stable and unstable manifolds intersect transversally. Such a transversal Intersection implies the appearance of Smale horseshoe-type chaotic dynamics that is similar to that in the periodically forced smooth systems. As an application, by using a combination of analytical and numerical methods, a quasiperiodically excited impact oscillator of Duffing type with two frequencies is studied in detail.

Keywords Impact oscillator · Quasiperiodic excitation · Melnikov method · Homoclinic bifurcation · Chaos

Mathematics Subject Classification 34C15 · 34G25 · 37C29

1 Introduction

Many problems from mechanics, electrical engineering, and control theory are modelled by piecewise smooth (PWS) dynamical systems. As a result, the study of bifurcation phenomena in those systems has become very popular in recent years. Like for smooth systems, it is very important to investigate the appearance of chaos for PWS systems. A typical route to chaos for PWS systems is through discontinuity-induced bifurcations, such as grazing, sliding, chattering, and border collision. There are many works on this subject. See, for example, the monographs [1–6] and the survey articles [7–12], and the references therein.

For many smooth systems, a common route to chaos is via homoclinic bifurcation. The Melnikov method is a powerful tool to deal with this kind of problems [4,13–19]. It is then natural to ask whether the Melnikov method established for smooth systems used to analyze subharmonic and homoclinic bifurcations can be extended to PWS systems. Many efforts have been made on this problem. To mention only a few of them, see [1,6,20–25]. All of those works assume that the unperturbed homoclinic or periodic orbit intersects the discontinuity surface transversally. In recent years, more attentions have been paid to the more interesting and difficult cases of bifurcations of sliding and grazing homoclinic orbits. In [4,26–29], Battelli, Fečkan, Awrejcewicz et al. extended the Melnikov method to bifurcation of sliding homoclinic orbits of general

J. Gao · Z. Du (✉)
Department of Mathematics, Sichuan University,
Chengdu 610064, Sichuan, People's Republic of China
e-mail: zdu1985@gmail.com

n-dimensional PWS systems, and for the first time, they show rigorously the existence of Smale horseshoe-type chaos in these systems. Grazing homoclinic bifurcation for a nonlinear inverted pendulum impacting between two rigid walls under external periodic excitation was also studied in [30].

Since many systems are externally excited by more than one frequency, systems under the action of quasiperiodic or almost periodic force are often encountered in real-world applications. Quasiperiodically forced smooth systems have been well studied in the past decades [17,31–35]. Particularly, in [17,31,32], Ide and Wiggins applied the Melnikov method to analyze homoclinic bifurcations of quasiperiodically forced smooth systems. However, although there has been big progress made in the study of homoclinic bifurcations in periodically forced PWS systems, little work has been done for quasiperiodically forced PWS systems. It is worth noting that in [36], Avramov and Awrejcewicz studied almost periodically forced frictional oscillations. They used the method of multiple scales to derive the modulation equations and constructed Melnikov function to study chaotic solutions of the system. In [4,20,21,27–29], Battelli and Fečkan investigated homoclinic bifurcations and chaos of quasiperiodically or almost periodically forced PWS systems.

A class of the most studied PWS systems is impact systems where a vibrator collides with one or more rigid walls or another moving object. Being typical PWS systems, impact oscillators are found in many mechanical systems, such as print hammers, rigid blocks, and walking machines. There are many interesting examples and applications of impact oscillators given in [2,5,6].

Motivated by the works of Ide and Wiggins [17, 31,32], Battelli and Fečkan [4,20,21,27–29], in this paper, we consider for the first time homoclinic bifurcation of the following quasiperiodically forced nonlinear impact system:

$$\begin{cases} \ddot{x} + g(x) = \varepsilon f(x, \dot{x}, t), & \text{as } |x| < 1, \\ \dot{x} \mapsto -(1 - \varepsilon\rho)\dot{x}, & \text{as } |x| = 1, \end{cases} \quad (1)$$

where $|\varepsilon| \leq \varepsilon_0 \ll 1$ for some $\varepsilon_0 > 0$ and the difference $1 - \varepsilon\rho \in (0, 1]$ is the coefficient of restitution representing energy loss during impact. System (1) can be used to model an inverted pendulum impacting on rigid walls as depicted in Fig. 1. Let $I = [-1, 1]$, $\mu > 0$ be a constant and $J_\mu = (-1 - \mu, 1 + \mu) \subset I$. Assume that functions f and g satisfy the following hypotheses:
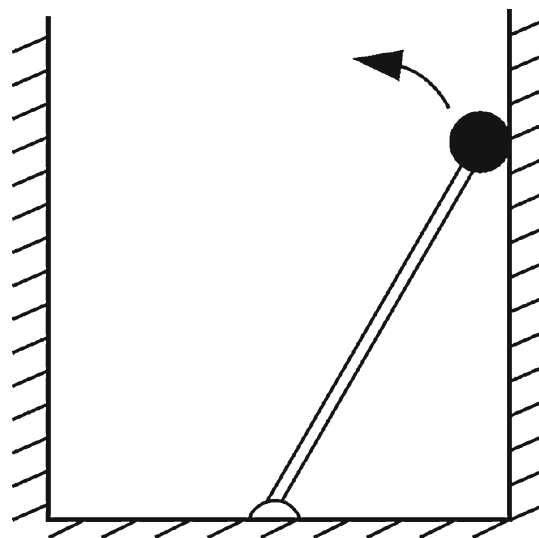
Fig. 1 Inverted pendulum

(H1) $g : J_\mu \rightarrow \mathbb{R}$ is C^2, where $g(0) = 0$, $g'(0) < 0$, $g(x) \neq 0$ for $x \in I - \{0\}$.

(H2) $f : J_\mu \times \mathbb{R} \times \mathbb{R} \rightarrow \mathbb{R}$ is C^2 and quasiperiodic in t with fundamental frequencies $\omega_1, \ldots, \omega_m$, where $m \geq 2$ is an integer. Hence, $f(x, y, t)$ can be written as $f(x, y, \theta_1, \ldots, \theta_m)$ with $\theta_k = \omega_k t$ for $1 \leq k \leq m$. Thus, for each fixed $(x, y) \in J_\mu \times \mathbb{R}$, $f(x, y, \theta_1, \ldots, \theta_m)$ is 2π-periodic in each of the θ_k coordinates for $1 \leq k \leq m$.

Let $\dot{x} = y$. For $\varepsilon = 0$, the unperturbed system describes a free impact oscillator and is equivalent to

$$\dot{x} = y, \quad \dot{y} = -g(x), \quad |x| < 1, \quad (2)$$

$$y \mapsto -y, \quad |x| = 1. \quad (3)$$

By Hypothesis (H1), system (2) has a unique equilibrium at the origin $O(0, 0)$ for $x \in I$, which is a saddle. Considering the identification given by the impact rule (3), the phase portrait of system (2–3) is qualitatively the same as shown in Fig. 2. Note that the unperturbed system (2–3) has a saddle at the origin O and two homoclinic loops $\Gamma_+ = OAA'O$ and $\Gamma_- = OBB'O$. Here, A', B' are the reflection points of A, B, respectively. Clearly, Γ_+ (respectively, Γ_-) intersects $x = +1$ (respectively, $x = -1$) transversally.

The impact inverted pendulum (1) was proposed by Chow et al. in [37,38]. It has been used in the modelling of many mechanical devices, such as rings, rigid standing structures, and a mooring buoy. Hence, periodically excited impact inverted pendulum has been extensively
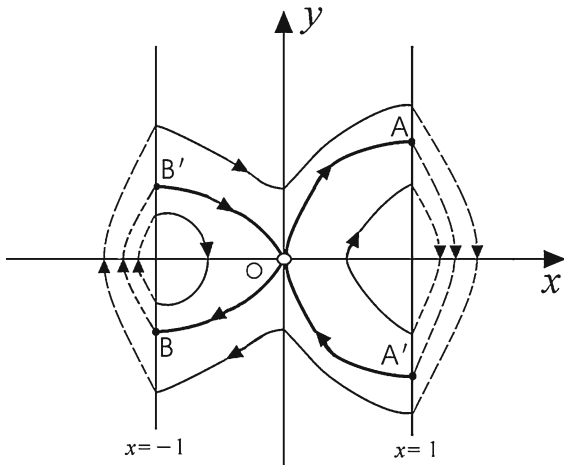
Fig. 2 Orbits of unperturbed system

studied for various choices of f and g [23,30,37–47]. In particular, in [23,45,46], the Melnikov methods for homoclinic and subharmonic bifurcations established for smooth systems were extended to be applicable to the nonlinear impact inverted pendulum. Grazing homoclinic bifurcation was also studied in [30]. However, to the best of our knowledge, there is still no result on the study of homoclinic bifurcation of quasiperiodically excited impact inverted pendulum in the literature. The purpose of this paper was to make some efforts on this problem.

More precisely, we discuss the perturbation of the homoclinic orbit Γ_+. The discussion for Γ_- is similar and is omitted for brevity. Let S^1 be the circle of period 2π, $T^m := S^1 \times \cdots \times S^1$ be the m-torus. Since system (1) is quasiperiodically excited, we consider the orbits of (1) and (2–3) in the region $|x| < 1$ in the space $\{(x, y) \mid |x| < 1, y \in \mathbb{R}\} \times T^m$. Then, system (2–3) has a normally hyperbolic m-torus $T_0 := \{(x, y) \in \mathbb{R}^2, (\theta_1, \ldots, \theta_m) \in T^m \mid (x, y) = (0, 0)\}$ whose right branch of $(m+1)$-dimensional stable manifold W_0^s and unstable manifold W_0^u coincide along the homoclinic manifold $\Gamma_+ \times T^m$. Then, for sufficiently small $|\varepsilon|$, the normally hyperbolic m-torus T_0 persists, which has a stable manifold W_ε^s and an unstable manifold W_ε^u. We are interested in the question: *under what conditions the perturbed stable manifold W_ε^s and unstable manifold W_ε^u intersect transversally?* By the generalization of the Smale–Birkhoff Homoclinic Theorem to the case of orbits homoclinic to normally hyperbolic invariant tori (Theorem 3.4.1 in [17, p. 322]), such a transversal intersection implies the appearance of chaotic dynam-

ics that is similar to the Smale horseshoe chaos in periodically forced system.

We extend the results for homoclinic bifurcation of quasiperiodically excited smooth systems obtained by Ide and Wiggins [17,31,32] to the general nonlinear quasiperiodically excited impact inverted pendulum (1). We present a method of Melnikov type to derive sufficient conditions under which the perturbed stable manifold W_ε^s and unstable manifold W_ε^u intersect transversally. Compare to the works [17,31,32], the main difficulty in our work is that, for system (1), in order to estimate the gap between W_ε^s and W_ε^u, we must estimate the time and velocity at which the orbit of (1) reaches the walls $|x| = 1$. This is overcome by using the perturbation method. As an application, by using a combination of analytical and numerical methods, a quasiperiodically excited impact inverted pendulum of Duffing type with two frequencies is studied in detail.

This paper is organized as follows. We introduce the Poincaré section and the Poincaré map for system (1) and present a method of Melnikov type to derive sufficient conditions under which W_ε^s and W_ε^u intersect transversally in Sect. 2. In Sect. 3, we apply this method to discuss the bifurcations of homoclinic loops for a quasiperiodically excited impact oscillator of Duffing type with two frequencies. Numerical simulations of this system are given in Sect. 4. Finally, discussion and some concluding remarks are given in Sect. 5.

2 Melnikov method

By (H2), for each fixed $(x, y) \in J_\mu \times \mathbb{R}$, $f(x, y, \theta_1, \theta_2, \ldots, \theta_m)$ can be viewed as a function on the m-torus T^m. Thus, system (1) is equivalent to the following suspended system

$$\left.\begin{aligned}
\dot{x} &= y \\
\dot{y} &= -g(x) + \varepsilon f(x, y, \theta_1, \ldots, \theta_m) \\
\dot{\theta}_1 &= \omega_1 \\
&\vdots \\
\dot{\theta}_m &= \omega_m
\end{aligned}\right\} \quad \text{as } |x| < 1,$$

(4)

$$y \mapsto -(1 - \varepsilon\rho)y \quad \text{as } |x| = 1,$$ (5)

where $(\theta_1, \ldots, \theta_m) \in T^m$. The solution of (4) with the initial conditions $x = x_0$, $y = y_0$, $\theta_1 = \theta_{10}, \ldots, \theta_m = \theta_{m0}$ is denoted by $x = x(t; x_0, y_0, \theta_{10}, \ldots, \theta_{m0})$,

$y = y(t; x_0, y_0, \theta_{10}, \ldots, \theta_{m0})$. For $\varepsilon = 0$, the unperturbed system is given by

$$\left.\begin{aligned} \dot{x} &= y \\ \dot{y} &= -g(x) \\ \dot{\theta}_1 &= \omega_1 \\ &\vdots \\ \dot{\theta}_m &= \omega_m \end{aligned}\right\} \quad \text{as } |x| < 1, \tag{6}$$

$$y \mapsto -y \quad \text{as } |x| = 1. \tag{7}$$

By (H1–H2), system (6–7) has a normally hyperbolic m-torus $T_0 := \{(x, y) \in \mathbb{R}^2, (\theta_1, \ldots, \theta_m) \in T^m \mid (x, y) = (0, 0)\}$ whose right branch of $(m + 1)$-dimensional stable and unstable manifolds W_0^s and W_0^u coincides along the homoclinic manifold $\Gamma_+ \times T^m$. By Proposition 4.1.5 in [17, p. 354], for sufficiently small ε, the perturbed system (4–5) has a normally hyperbolic m-torus T_ε, which has $(m + 1)$-dimensional C^2 stable and unstable manifolds W_ε^s and W_ε^u.

Because of the nature of the vector field (4–5), in order to study the perturbation of the right homoclinic orbit Γ_+, the Poincaré section is taken to be the following set

$$\begin{aligned} \Sigma = \{(x, y, \theta_1, \ldots, \theta_m) &\in I \times \mathbb{R} \times S^1 \times \cdots \times S^1 \mid \\ x = 1, y > 0\} &= \mathbb{R}^+ \times T^m. \end{aligned}$$

Let

$$\begin{aligned} \Sigma_- = \{(x, y, \theta_1, \ldots, \theta_m) &\in I \times \mathbb{R} \times S^1 \times \cdots \times S^1 \mid \\ x = 1, y < 0\} &= \mathbb{R}^- \times T^m. \end{aligned}$$

Elements in both Σ and Σ_- are denoted by $(y, \theta_1, \ldots, \theta_m)$. The Poincaré map $\mathscr{P} : \Sigma \mapsto \Sigma$ is defined as follows. Consider a point $(y_0, \Theta_0) \in \Sigma$, where $\Theta_0 := (\theta_{10}, \ldots, \theta_{m0})$. It is immediately mapped to $(-(1 - \varepsilon\rho)y_0, \Theta_0) \in \Sigma_-$ by the impact law (5). Then, under the flow of system (4), it returns to Σ after a free flight of duration $\tau(y_0, \Theta_0)$. Then,

$$\begin{aligned} \mathscr{P}(y_0, \Theta_0) = (&y(\tau(y_0, \Theta_0); 1, -(1 - \varepsilon\rho)y_0, \Theta_0), \\ &(\omega_1 \tau(y_0, \Theta_0) + \theta_{10})(\text{mod } T_1), \\ &\ldots, (\omega_m \tau(y_0, \Theta_0) + \theta_{m0})(\text{mod } T_m)), \end{aligned}$$

where $T_i = 2\pi/\omega_i$ for $i = 1, \ldots, m$.

For any $(\theta_{10}, \ldots, \theta_{m0}) \in T^m$ and sufficiently small ε, a branch of the unstable (respectively, stable) manifold W_ε^u (respectively, W_ε^s) intersects Σ (resp. Σ_-) in a m-dimensional manifold, denoted by $\Delta_\varepsilon^u(\theta_{10}, \ldots, \theta_{m0})$ (respectively, $\Delta_\varepsilon^s(\theta_{10}, \ldots, \theta_{m0})$). The point $(\theta_{10}, \ldots, \theta_{m0}) \in T^m$ can be viewed as parameters along the unperturbed homoclinic manifold

$\Gamma_+ \times T^m$. Moreover, the impact rule (5) defines a 1–1 map $\mathscr{I} : \Sigma \to \Sigma_-$ such that

$$(y, \theta_1, \ldots, \theta_m) \mapsto (-(1 - \varepsilon\rho)y, \theta_1, \ldots, \theta_m).$$

Hence, the manifold $\Delta_\varepsilon^s(\theta_{10}, \ldots, \theta_{m0})$ is the image of the map $\mathscr{I}$ of the manifold $-(1 - \varepsilon\rho)^{-1} \Delta_\varepsilon^s(\theta_{10}, \ldots, \theta_{m0})$ on Σ. The *separation* between W_ε^s and W_ε^u in Σ is given by

$$\begin{aligned} \Delta_\varepsilon(\theta_{10}, \ldots, \theta_{m0}) = &\Delta_\varepsilon^u(\theta_{10}, \ldots, \theta_{m0}) \\ &+ \frac{1}{1 - \varepsilon\rho} \Delta_\varepsilon^s(\theta_{10}, \ldots, \theta_{m0}), \quad (8) \end{aligned}$$

where $(\theta_{10}, \ldots, \theta_{m0}) \in T^m$. If $\Delta_\varepsilon(\theta_{10}, \ldots, \theta_{m0})$ has no zeros, then W_ε^s and W_ε^u do not intersect, while if $\Delta_\varepsilon(\theta_{10}, \ldots, \theta_{m0})$ has simple zeros, then W_ε^s and W_ε^u intersect transversally. If $\Delta_\varepsilon(\theta_{10}, \ldots, \theta_{m0})$ has quadratic zeros, then W_ε^s and W_ε^u intersect with quadratic tangencies. By the generalization of the Smale–Birkhoff Homoclinic Theorem to the case of orbits homoclinic to normally hyperbolic invariant tori (Theorem 3.4.1 in [17, p. 322]), if W_ε^s intersects W_ε^u transversally, then the Poincaré map $\mathscr{P} : \Sigma \mapsto \Sigma$ possesses transversal homoclinic torus, implying the appearance of chaotic dynamics that is similar to the Smale horseshoe chaos in periodically forced system.

Usually, it is impossible to find a closed form of the separation $\Delta_\varepsilon(\theta_{10}, \ldots, \theta_{m0})$. It has to be approximated by perturbation methods. Since W_ε^s and W_ε^u are C^2 in ε under Hypotheses (H1) and (H2), $\Delta_\varepsilon^u(\theta_{10}, \ldots, \theta_{m0})$, $\Delta_\varepsilon^s(\theta_{10}, \ldots, \theta_{m0})$ and $\Delta_\varepsilon(\theta_{10}, \ldots, \theta_{m0})$ are all C^2 in ε from the way they are defined. Suppose that $\Delta_\varepsilon^u(\theta_{10}, \ldots, \theta_{m0})$ and $\Delta_\varepsilon^s(\theta_{10}, \ldots, \theta_{m0})$ have the following Taylor expansions near $\varepsilon = 0$:

$$\begin{aligned} \Delta_\varepsilon^u(\theta_{10}, \ldots, \theta_{m0}) = &M_0^u(\theta_{10}, \ldots, \theta_{m0}) \\ &+ M_1^u(\theta_{10}, \ldots, \theta_{m0})\varepsilon + O(\varepsilon^2), \end{aligned}$$
$$\tag{9}$$

$$\begin{aligned} \Delta_\varepsilon^s(\theta_{10}, \ldots, \theta_{m0}) = &M_0^s(\theta_{10}, \ldots, \theta_{m0}) \\ &+ M_1^s(\theta_{10}, \ldots, \theta_{m0})\varepsilon + O(\varepsilon^2). \end{aligned}$$
$$\tag{10}$$

Clearly $M_0^u(\theta_{10}, \ldots, \theta_{m0}) \equiv -M_0^s(\theta_{10}, \ldots, \theta_{m0}) \equiv \sqrt{-2G(1)}$, where

$$G(x) := \int_0^x g(s)\mathrm{d}s, \quad x \in J.$$

Hence, from (8)–(10), we obtain

$$\Delta_\varepsilon(\theta_{10}, \ldots, \theta_{m0}) = M_1(\theta_{10}, \ldots, \theta_{m0})\varepsilon + O(\varepsilon^2),$$
$$\tag{11}$$

where $M_1(\theta_{10}, \ldots, \theta_{m0})$ is called the first-order Melnikov function and is given by

$$M_1(\theta_{10}, \ldots, \theta_{m0}) = -\rho\sqrt{-2G(1)} + M_1^u(\theta_{10}, \ldots, \theta_{m0}) + M_1^s(\theta_{10}, \ldots, \theta_{m0}). \quad (12)$$

Similar to Theorem 2.2 of [32], we obtain the following result:

Theorem 1 *Let ∇M_1 be the gradient of $M_1(\theta_{10}, \ldots, \theta_{m0})$. If $M_1(\theta_{10}, \ldots, \theta_{m0})$ has a simple zero $(\bar{\theta}_{10}, \ldots, \bar{\theta}_{m0})$, namely $M_1(\bar{\theta}_{10}, \ldots, \bar{\theta}_{m0}) = 0$ and $\nabla M_1(\bar{\theta}_{10}, \ldots, \bar{\theta}_{m0}) \neq 0$, then for sufficiently small $\varepsilon > 0$, the perturbed manifolds W_ε^s and W_ε^u intersect transversally in Σ near $(\bar{\theta}_{10}, \ldots, \bar{\theta}_{m0})$. Furthermore, if $\nabla M_1(\theta_{10}, \ldots, \theta_{m0}) \neq 0$ for all $(\theta_{10}, \ldots, \theta_{m0}) \in T^m$, then this zero of $M_1(\theta_{10}, \ldots, \theta_{m0})$ can be continued to a m-dimensional transverse homoclinic torus.*

Now, we describe how to compute the first-order Melnikov function $M_1(\theta_{10}, \ldots, \theta_{m0})$. Select P_0^u: $(x_0^u(0), y_0^u(0))$ and P_0^s: $(x_0^s(0), y_0^s(0))$ on the unperturbed (i.e., $\varepsilon = 0$) unstable manifold W_0^u and stable manifold W_0^s of the saddle O of (4), respectively, such that $0 < x_0^u(0) < \mu$, $0 < x_0^s(0) < \mu$. Let γ_0^u : $(x_0^u(t), y_0^u(t))$ and γ_0^s : $(x_0^s(t), y_0^s(t))$ denote the orbits of (4) for $\varepsilon = 0$ passing through P_0^u and P_0^s at $t = 0$, respectively, which of course lie in W_0^u and W_0^s, respectively. Let τ_0^u and τ_0^s be the time at which the orbits γ_0^u, γ_0^s reach the wall $x = 1$, respectively, i.e., $x_0^s(\tau_0^s) = x_0^u(\tau_0^u) = 1$. Clearly, when $1 < x_0^u(0) < \mu$ and $1 < x_0^s(0) < \mu$, we have $\tau_0^u < 0$ and $\tau_0^s > 0$; when $0 < x_0^u(0) \leq 1$ and $0 < x_0^s(0) \leq 1$, we have $\tau_0^u \geq 0$ and $\tau_0^s \leq 0$. Then, similar to the derivation given in [23], we obtain

Theorem 2 *Let $x_0^u, y_0^u, x_0^s, y_0^s$ and τ_0^u, τ_0^s be given above. Then, the first-order Melnikov function $M_1(\theta_{10}, \ldots, \theta_{m0})$ is calculated by*

$$M_1(\theta_{10}, \ldots, \theta_{m0}) = -\rho\sqrt{-2G(1)} + \frac{1}{\sqrt{-2G(1)}}$$
$$\left\{ \int_{-\infty}^{\tau_0^u} F^u(\tau, \Theta_0) \mathrm{d}\tau + \int_{\tau_0^s}^{+\infty} F^s(\tau, \Theta_0) \mathrm{d}\tau \right\},$$
where

$$F^u(\tau, \Theta_0) = f\left(x_0^u(\tau), y_0^u(\tau), \omega_1(\tau - \tau_0^u) + \theta_{10}, \ldots, \omega_m(\tau - \tau_0^u) + \theta_{m0}\right) y_0^u(\tau),$$
$$F^s(\tau, \Theta_0) = f\left(x_0^s(\tau), y_0^s(\tau), \omega_1(\tau - \tau_0^s) + \theta_{10}, \ldots, \omega_m(\tau - \tau_0^s) + \theta_{m0}\right) y_0^s(\tau).$$

The proof for Theorem 2 is similar to the proof for Theorem 3.1 in [23] and thus is omitted here for brevity.

3 Impact duffing system

It is well known that Duffing's equation has been found in many mechanical problems [15, p. 82]. Thus, naturally we consider the following quasiperiodically forced impact Duffing system with two fundamental frequencies:

$$\begin{cases} \ddot{x} + \varepsilon\delta\dot{x} - x + x^3 = \varepsilon \sum_{k=1}^{2} \gamma_k \cos\omega_k t, & |x| < 1, \\ \dot{x} \mapsto -(1 - \varepsilon\rho)\dot{x}, & |x| = 1, \end{cases} \quad (13)$$

where $\varepsilon \geq 0, \delta \geq 0, \gamma_1, \gamma_2 > 0, \omega_1, \omega_2 > 0$ and $\rho \geq 0$. Let $y = \dot{x}$, system (13) is equivalent to the following system

$$\begin{cases} \dot{x} = y \\ \dot{y} = x - x^3 + \varepsilon\left(-\delta y + \sum_{k=1}^{2} \gamma_k \cos\omega_k t\right), \end{cases} \quad \text{as } |x| < 1, \quad (14)$$

$$y \mapsto -(1 - \varepsilon\rho)y, \quad \text{as } |x| = 1. \quad (15)$$

When $\varepsilon = 0$, the phase portrait of the unperturbed system of (14–15) is topologically equivalent to that shown in Fig. 2. Take

$$\left(x_0^u(t), y_0^u(t)\right) = \left(\sqrt{2}\mathrm{sech}\, t, -\sqrt{2}\mathrm{sech}\, t \tanh t\right), \quad t \in (-\infty, 0],$$
$$\left(x_0^s(t), y_0^s(t)\right) = \left(\sqrt{2}\mathrm{sech}\, t, -\sqrt{2}\mathrm{sech}\, t \tanh t\right), \quad t \in [0, +\infty).$$

Let $\kappa = \ln(\sqrt{2} + 1)$. Then, $\tau_0^u = -\kappa$, $\tau_0^s = \kappa$. By Theorem 2, we have

$$M_1(\theta_{10}, \theta_{20}) = -\frac{\rho}{\sqrt{2}} - \frac{2\delta}{3}\left(2\sqrt{2} - 1\right)$$
$$+ 4\gamma_1 I(\omega_1)\sin\theta_{10}$$
$$+ 4\gamma_2 I(\omega_2)\sin\theta_{20}, \quad (16)$$

where $\theta_{10}, \theta_{20} \in [0, 2\pi]$ and

$$I(\omega) = \omega \int_0^{+\infty} \mathrm{sech}\,(t + \kappa)\cos(\omega t)\mathrm{d}t.$$

From (16), it is clear that if

$$\frac{\rho}{\sqrt{2}} + \frac{2\delta}{3}\left(2\sqrt{2} - 1\right) < 4\gamma_1 I(\omega_1) + 4\gamma_2 I(\omega_2),$$

then the first-order Melnikov function $M_1(\theta_{10}, \theta_{20})$ has a simple zero. Thus, in the six-dimensional parameter space $(\rho, \delta, \gamma_1, \gamma_2, \omega_1, \omega_2)$, the bifurcation set is given by the five-dimensional surface

$$\frac{\rho}{\sqrt{2}} + \frac{2\delta}{3}\left(2\sqrt{2} - 1\right) = 4\gamma_1 I(\omega_1) + 4\gamma_2 I(\omega_2). \quad (17)$$

Since the left side of (17) is a linear combination of ρ and δ with constant coefficients, without the loss of
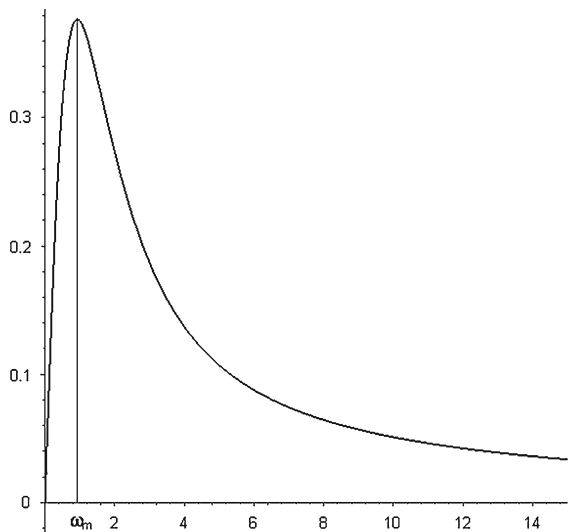
Fig. 3 Graph of $I(\omega)$ for $\omega > 0$. ω_m is the unique maximum of $I(\omega)$

generality, let $\alpha := \frac{\rho}{\sqrt{2}} + \frac{2\delta}{3}(2\sqrt{2} - 1)$, $I_1 := I(\omega_1)$ and $I_2 := I(\omega_2)$ in the rest of the paper. Then, (17) can be rewritten in the following form

$$-\frac{1}{4}\alpha + \gamma_1 I_1 + \gamma_2 I_2 = 0. \tag{18}$$

As shown in Fig. 3, the function $I(\omega)$ has a unique maximum $\omega_m \approx 0.930895866$ with $I_m := I(\omega_m) \approx 0.376828848$. Furthermore, $I(\omega)$ is strictly increasing for $\omega \in (0, \omega_m)$ and strictly decreasing for $\omega \in (\omega_m, +\infty)$. If $\alpha > 4(\gamma_1 + \gamma_2)I_m$, then $M_1(\theta_{10}, \theta_{20}) < 0$, implying that for sufficiently small $\varepsilon > 0$, W_ε^s and W_ε^u do not intersect. If $\alpha = 4(\gamma_1 + \gamma_2)I_m$, then $M_1(\theta_{10}, \theta_{20})$ has a unique zero $\theta_{10} = \theta_{20} = \frac{\pi}{2}$ if and only if $\omega_1 = \omega_2 = \omega_m$. Furthermore, if $\omega_1 = \omega_2 = \omega_m$, then $\nabla M_1(\frac{\pi}{2}, \frac{\pi}{2}) = 0$.

In the rest of the paper, we focus our attention on the case $\alpha < 4(\gamma_1 + \gamma_2)I_m$. Clearly, for a given value of $(\alpha, \gamma_1, \gamma_2)$, points in the $I_1 - I_2$ plane above the line segment given by (18) inside the rectangle $\mathscr{D} := \{(I_1, I_2) \in \mathbb{R}^2 \mid 0 \le I_1, I_2 \le I_m\}$ correspond to transverse homoclinic tori. Let $\omega^+(I)$ (respectively, $\omega^-(I)$) be the inverse function of $I(\omega)$ for $\omega \in (0, \omega_m)$ (respectively, $\omega \in (\omega_m, +\infty)$). In the following, we use the same method in [32] to represent the bifurcation sets for the case $\alpha < 4(\gamma_1 + \gamma_2)I_m$ in the $\omega_1 - \omega_2$ plane. Our discussion can be divided into nine cases as follows, where for each case in the diagram of the

corresponding bifurcation set, the shaded area corresponds to transverse homoclinic tori. Parameters chosen from this area correspond to the chaotic behavior of system (13), thus the area is called *chaotic zone*.

(1) If $4I_m \max\{\gamma_1, \gamma_2\} < \alpha < 4(\gamma_1 + \gamma_2)I_m$, then the line (18) intersects $\partial\mathscr{D}$ at (I_{h1}, I_m) and (I_m, I_{v1}) with $0 < I_{h1}, I_{v1} < I_m$, where $\partial\mathscr{D}$ is the boundary of $\mathscr{D}$ and

$$I_{h1} = \frac{1}{\gamma_1}\left(\frac{1}{4}\alpha - \gamma_2 I_m\right), \quad I_{v1} = \frac{1}{\gamma_2}\left(\frac{1}{4}\alpha - \gamma_1 I_m\right).$$

The corresponding bifurcation set in the $\omega_1 - \omega_2$ plane is given in Fig. 4a. The corresponding chaotic zone is denoted by $\mathscr{C}_1$.

(2) If $\gamma_1 > \gamma_2$ and $\alpha = 4I_m \max\{\gamma_1, \gamma_2\} = 4\gamma_1 I_m$, then the line (18) intersects $\partial\mathscr{D}$ at $(I_m, 0)$ and (I_{h2}, I_m) with $0 < I_{h2} = I_m(\gamma_1 - \gamma_2)/\gamma_1 < I_m$. The corresponding bifurcation set in the $\omega_1 - \omega_2$ plane is given in Fig. 4b. The corresponding chaotic zone is denoted by $\mathscr{C}_2$.

(3) If $\gamma_1 < \gamma_2$ and $\alpha = 4I_m \max\{\gamma_1, \gamma_2\} = 4\gamma_2 I_m$, then the line (18) intersects $\partial\mathscr{D}$ at $(0, I_m)$ and (I_m, I_{v3}) with $0 < I_{v3} = I_m(\gamma_2 - \gamma_1)/\gamma_2 < I_m$. The corresponding bifurcation set in the $\omega_1 - \omega_2$ plane is given in Fig. 4c. The corresponding chaotic zone is denoted by $\mathscr{C}_3$.

(4) If $\gamma_1 = \gamma_2$ and $\alpha = 4I_m \max\{\gamma_1, \gamma_2\} = 4\gamma_2 I_m = 4\gamma_1 I_m$, then the line (18) intersects $\partial\mathscr{D}$ at $(0, I_m)$ and $(I_m, 0)$. The corresponding bifurcation set in the $\omega_1 - \omega_2$ plane is given in Fig. 4d. The corresponding chaotic zone is denoted by $\mathscr{C}_4$.

(5) If $\gamma_1 > \gamma_2$ and $4\gamma_2 I_m < \alpha < 4\gamma_1 I_m$, then the line (18) intersects $\partial\mathscr{D}$ at $(I_{h5A}, 0)$ and (I_{h5B}, I_m) with $0 < I_{h5A} = \frac{\alpha}{4\gamma_1}$, $I_{h5B} = I_{h1} < I_m$. The corresponding bifurcation set in the $\omega_1 - \omega_2$ plane is given in Fig. 4e. The corresponding chaotic zone is denoted by $\mathscr{C}_5$.

(6) If $\gamma_1 < \gamma_2$ and $4\gamma_1 I_m < \alpha < 4\gamma_2 I_m$, then the line (18) intersects $\partial\mathscr{D}$ at $(0, I_{v6A})$ and (I_m, I_{v6B}) with $0 < I_{v6A} = \frac{\alpha}{4\gamma_2}$, $I_{v6B} = I_{v1} < I_m$. The corresponding bifurcation set in the $\omega_1 - \omega_2$ plane is given in Fig. 4f. The corresponding chaotic zone is denoted by $\mathscr{C}_6$.

(7) If $\gamma_1 > \gamma_2$ and $\alpha = 4I_m \min\{\gamma_1, \gamma_2\} = 4\gamma_2 I_m$, then the line (18) intersects $\partial\mathscr{D}$ at $(0, I_m)$ and $(I_{h7}, 0)$ with $0 < I_{h7} = \frac{\gamma_2}{\gamma_1}I_m < I_m$. The corresponding bifurcation set in the $\omega_1 - \omega_2$ plane is given in
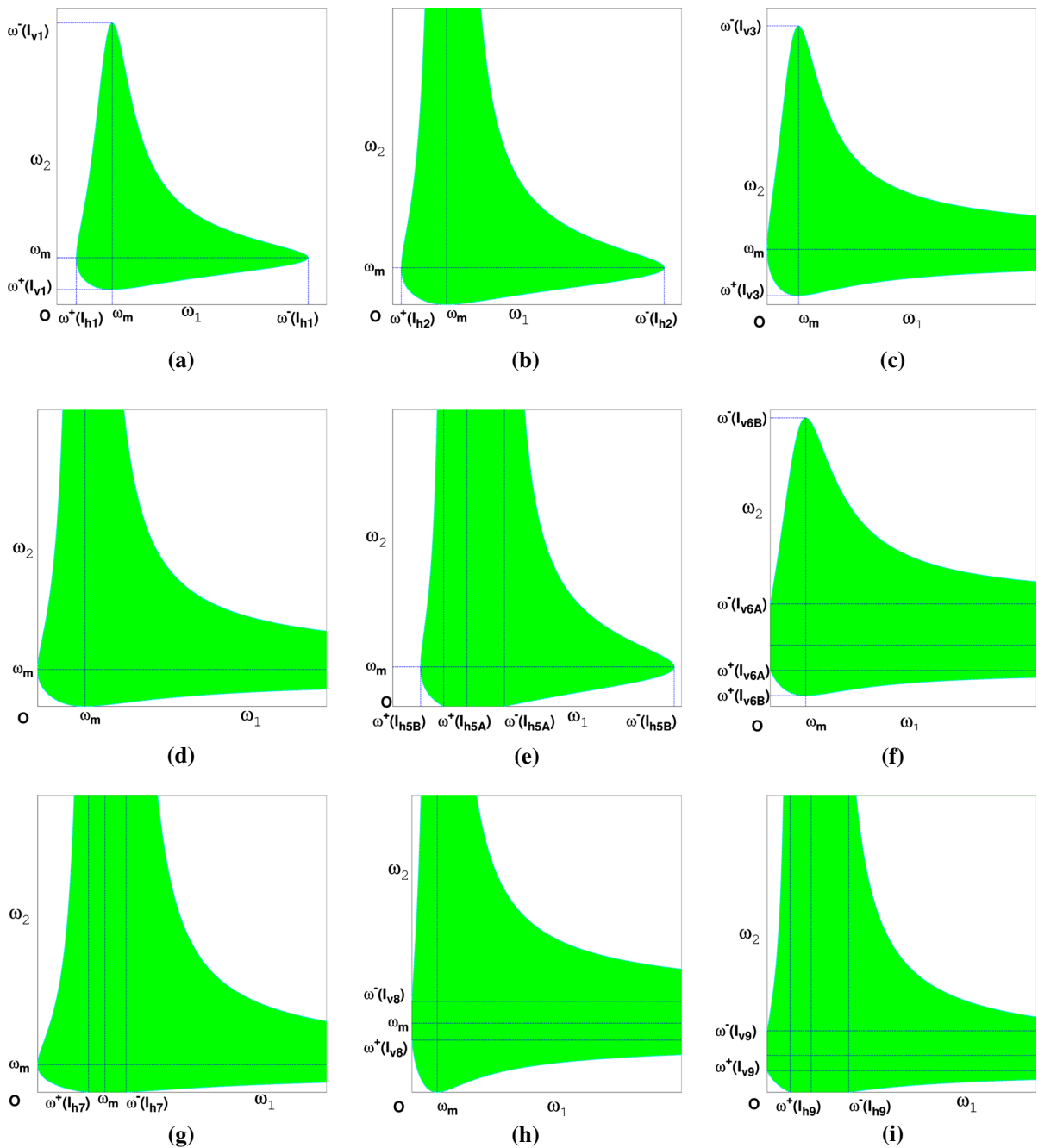
Fig. 4 Bifurcation sets in $\omega_1 - \omega_2$ plane, the shaded area corresponds to transverse homoclinic tori. **a** $4I_m \max\{\gamma_1, \gamma_2\} < \alpha < 4(\gamma_1 + \gamma_2)I_m$. **b** $\gamma_1 > \gamma_2$ and $\alpha = 4\gamma_1 I_m$. **c** $\gamma_1 > \gamma_2$ and $\alpha = 4\gamma_1 I_m$. **d** $\gamma_1 = \gamma_2$ and $\alpha = 4\gamma_1 I_m$. **e** $\gamma_1 > \gamma_2$ and $4\gamma_2 I_m < \alpha < 4\gamma_1 I_m$. **f** $\gamma_1 < \gamma_2$ and $4\gamma_1 I_m < \alpha < 4\gamma_2 I_m$. **g** $\gamma_1 > \gamma_2$ and $\alpha = 4\gamma_2 I_m$. **h** $\gamma_1 < \gamma_2$ and $\alpha = 4\gamma_1 I_m$. **i** $0 < \alpha < 4I_m \min\{\gamma_1, \gamma_2\}$.

Fig. 4g. The corresponding chaotic zone is denoted by $\mathscr{C}_7$.

(8) If $\gamma_1 < \gamma_2$ and $\alpha = 4I_m \min\{\gamma_1, \gamma_2\} = 4\gamma_1 I_m$, then the line (18) intersects $\partial\mathscr{D}$ at $(I_m, 0)$ and $(0, I_{v8})$

with $0 < I_{v8} = \frac{\gamma_1}{\gamma_2} I_m < I_m$. The corresponding bifurcation set in the $\omega_1 - \omega_2$ plane is given in Fig. 4h. The corresponding chaotic zone is denoted by $\mathscr{C}_8$.
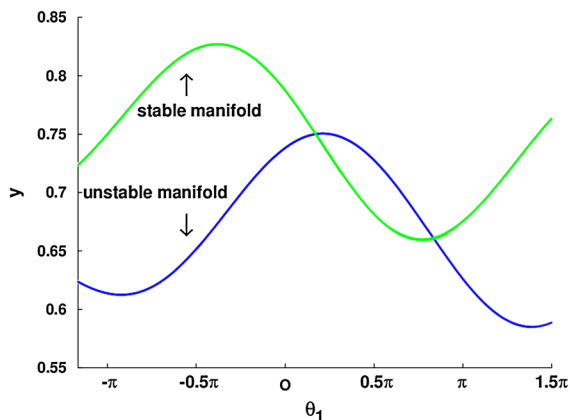
Fig. 5 The intersections of W_ε^u and W_ε^s in $\Sigma_{\theta_{1m},\theta_{1M}}^{\theta_{20*}}$, where $\gamma_1 = 1.1$, $\gamma_2 = 1.0$, $\omega_1 = \frac{\pi}{3}$, $\omega_2 = 0.7$, $\varepsilon = 0.04$, $\delta = 1.6$, $\rho = 0$, $[\theta_{1m}, \theta_{1M}] = [-\frac{7}{6}\pi, \frac{3}{2}\pi]$ and $\theta_{20*} = 0.5\pi$

(9) If $0 < \alpha < 4I_m \min\{\gamma_1, \gamma_2\}$, then the line (18) intersects $\partial \mathcal{D}$ at $(I_{h9}, 0)$ and $(0, I_{v9})$ with $0 < I_{h9} = \frac{\alpha}{4\gamma_1}$, $I_{v9} = \frac{\alpha}{4\gamma_2} < I_m$. The corresponding bifurcation set in the $\omega_1 - \omega_2$ plane is given in Fig. 4i. The corresponding chaotic zone is denoted by $\mathscr{C}_9$.

4 Numerical simulations

In this section, we present numerical simulations for the impact Duffing system (13) to show the theoretical results from the Melnikov method in Sect. 3. It is easy to see that for the nine bifurcation sets described in Sect. 3, by switching the roles of γ_1 and γ_2, cases (3), (6), and (8) are the same as cases (2), (5), and (7), respectively. Thus, we omit cases (3), (6), and (8) in the numerical simulations for brevity. The computations are implemented in MATLAB.

When performing numerical simulations for system (13), it is important and difficult to detect the impacting time and velocity accurately. We adopt an event-driven method described in [2,48] for this purpose. We implement this method by using the built-in event detection routines along with the built-in ODE solvers of MATLAB. In this way, we are able to detect the impacting events as accurate as the accuracy of MATLAB allows as suggested by Piiroinen and Kuznetsov in [48].

We first describe how to plot the intersections of the perturbed unstable manifold W_ε^u and stable manifold W_ε^s in a fixed slice of the Poincaré section Σ given by

$$\Sigma_{\theta_{1m},\theta_{1M}}^{\theta_{20*}} = \{(y, \theta_1, \theta_2) \in \Sigma \mid \theta_1 \in [\theta_{1m}, \theta_{1M}], \theta_2 = \theta_{20*}\},$$

where θ_{1m}, θ_{1M}, and θ_{20*} are constants, $\theta_{1M} - \theta_{1m} \geq T_1$. For this purpose, we modified the method for the computation of stable and unstable manifolds of hyperbolic trajectories in two-dimensional aperiodically time-dependent systems proposed by Mancho et al. [49] so it is applicable to system (13). The algorithm is described as follows.

The first step is to find the *distinguished hyperbolic trajectory* $\xi_{DHT}(t, \varepsilon) := (x_{DHT}(t, \varepsilon), y_{DHT}(t, \varepsilon))$ of system (13) (see [49] for the definition), which is the unique quasiperiodic orbit of (13) such that $\xi_{DHT}(t, \varepsilon) \to (0, 0)$ uniformly for $t \in (-\infty, +\infty)$ as $\varepsilon \to 0$. Thus we have

$$\xi_{DHT}(t, \varepsilon) = \varepsilon \sum_{k=1}^{2} \frac{\gamma_k}{1 + \omega_k^2} (-\cos \omega_k t, \omega_k \sin \omega_k t) + \varepsilon^2$$
$$\sum_{k=1}^{2} \frac{\delta \gamma_k \omega_k}{(1 + \omega_k^2)^2} (\sin \omega_k t, \omega_k \cos \omega_k t) + O(\varepsilon^3).$$

The second step is to approximate the local stable and unstable manifolds. As described in [49], they are given by the straight line segment between $\xi_{DHT}(t, \varepsilon)$ and
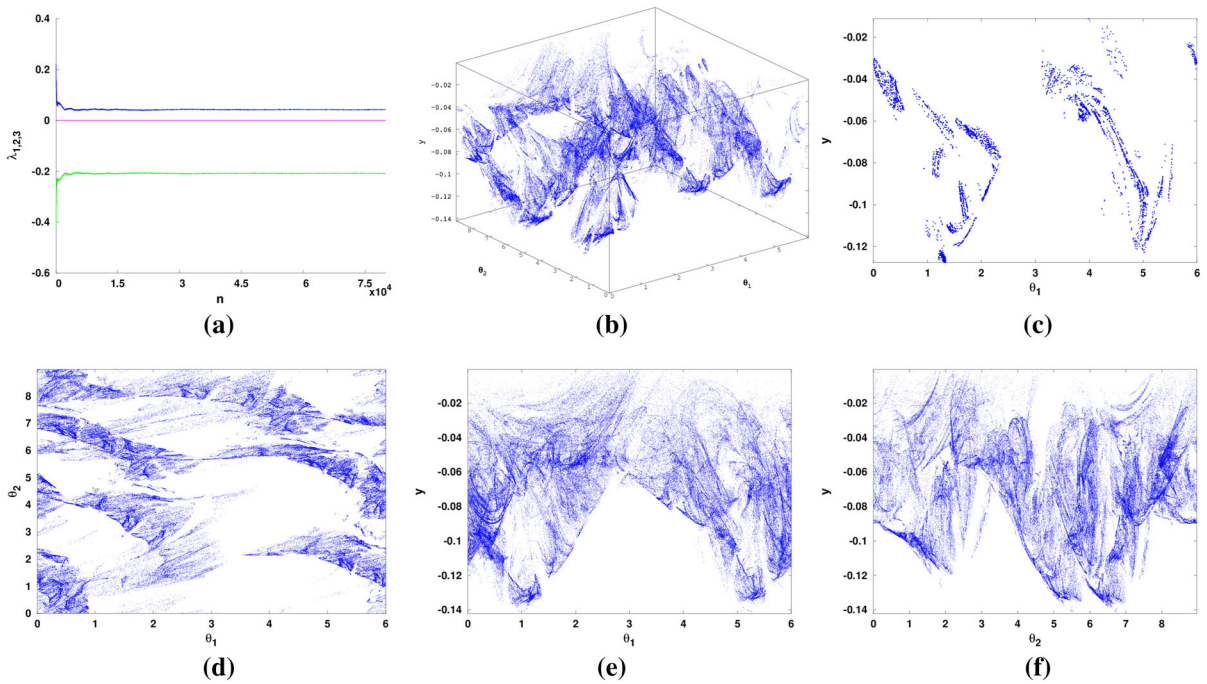
Table 1 Parameters for numerical simulation and the largest Lyapunov exponent λ_{max}, where $\gamma_m \approx 1.293904566$. The other parameters are fixed as $\rho = 0$, $\varepsilon = 0.04$, $\delta = 1.6$ and $\omega_1 = \frac{\pi}{3}$

Chaotic zone	γ_1	γ_2	ω_2	$\bar{\theta}_{10}$	$\bar{\theta}_{20}$	θ_{20}	$\Delta\theta_2$	λ_{max}
$\mathscr{C}_1$	1.1	1	0.7	0.5π	0.5π	5.9	0.1	0.042
$\mathscr{C}_2$	γ_m	1	0.5	0.5π	1.6	6.0	0.15	0.046
$\mathscr{C}_4$	γ_m	γ_m	0.5	$\frac{\pi}{7}$	1	6.5	0.15	0.038
$\mathscr{C}_5$	1.5	1	0.4	0.5π	0.5π	6.6	0.3	0.066
$\mathscr{C}_7$	1.5	γ_m	0.3	0.4π	1.55	18.8	0.3	0.048
$\mathscr{C}_9$	1.6	1.5	0.3	$\frac{\pi}{3}$	1.5	12.55	0.25	0.073

Fig. 6 Parameters are chosen from $\mathscr{C}_1$ with $\gamma_1 = 1.1$, $\gamma_2 = 1$, $\omega_2 = 0.7$ and $\bar{\theta}_{10} = \bar{\theta}_{20} = 0.5\pi$. **a** Convergent sequences of the Lyapunov exponents, **b** the Poincaré map, **c** a projection of the double Poincaré map on to the (θ_1, y) plane, **d** a projection of the Poincaré map on to the (θ_1, θ_2) plane and **e** on to the (θ_1, y) plane and **f** on to the (θ_2, y) plane.

$$\xi_W^{u,s}(t, \varepsilon) = \xi_{DHT}(t, \varepsilon) + \frac{1}{\sqrt{2}}\lambda \left(e^{u,s}(t) + O(\varepsilon^2) \right),$$

where $e^u(t) = (1, 1)$, $e^s(t) = (-1, 1)$, λ is a parameter that can be adjusted if necessary during the computation. In the third step, the interval $[\theta_{1m}, \theta_{1M}]$ is partitioned equally into N parts by $\theta_{1m} = \theta_1^0 < \theta_1^2 < \cdots < \theta_1^N = \theta_{1M}$, where N is a sufficiently large positive integer. Then, for each θ_1^j ($0 \leq j \leq N$), we apply the method described in [49] to compute W_ε^u and W_ε^s in the time slice

$$\Pi_{\theta_1^j} := \left\{ (x, y, t) \in \mathbb{R}^3 \mid t = \theta_1^j \right\}$$

until $x = 1$, and we obtain a point $(1, y_{\theta_1^j}, \theta_1^j) \in \Pi_{\theta_1^j}$. Consequently, for W_ε^u, we obtain a point $(y_{\theta_1^j}, \theta_1^j, \theta_{20*})$ $\in \Sigma_{\theta_{1m}, \theta_{1M}}^{\theta_{20*}}$; for W_ε^s, applying the impact law (15), we obtain a point $(-(1 - \varepsilon\rho)^{-1} y_{\theta_1^j}, \theta_1^j, \theta_{20*})$ $\in$ $\Sigma_{\theta_{1m}, \theta_{1M}}^{\theta_{20*}}$. By this method, we in fact approximated the curves $\Delta_\varepsilon^u(\theta_1, \theta_{20*})$ and $\Delta_\varepsilon^s(\theta_1, \theta_{20*})$ defined in Sect. 2. Clearly, if $\Delta_\varepsilon^u(\theta_1, \theta_{20*})$ and $\Delta_\varepsilon^s(\theta_1, \theta_{20*})$ intersect transversally, then the two surfaces $\Delta_\varepsilon^u(\theta_1, \theta_2)$ and $\Delta_\varepsilon^s(\theta_1, \theta_2)$ also intersect transversally, implying that W_ε^u and W_ε^s intersect transversally.

For the sake of brevity, we only show one instance of the computation. Take $\gamma_1 = 1.1$, $\gamma_2 = 1.0$, $\omega_1 = \frac{\pi}{3}$, $\omega_2 = 0.7$, $\varepsilon = 0.04$, $\delta = 1.6$, $\rho = 0$, $[\theta_{1m}, \theta_{1M}] = [-\frac{7}{6}\pi, \frac{3}{2}\pi]$, $\theta_{20*} = 0.5\pi$. It is easy to check that the parameters are in the chaotic zone $\mathscr{C}_1$, and the result is shown in Fig. 5. As can be seen that the two curves $\Delta_\varepsilon^u(\theta_1, \theta_{20*})$ and $\Delta_\varepsilon^s(\theta_1, \theta_{20*})$ intersect transversally at $\theta_1 \approx 0.5389$ and $\theta_1 \approx 2.6233$, implying that W_ε^u and W_ε^s intersect transversally. Hence, the result confirms the theoretical prediction given in Sect. 3.

As pointed out in [33] and [35], since the Poincaré map for system (13) is a three-dimensional map, the fractal nature of the strange attractor of the map, if it exits, is not evident. We adopt the double Poincaré section technique proposed by Moon and Holmes in [33] to overcome this difficulty as follows. Take a thin section

$$\Sigma^{\theta_{20}, \Delta\theta_2} = \{(y, \theta_1, \theta_2) \in \Sigma \mid \theta_2 \in [\theta_{20}, \theta_{20} + \Delta\theta_2]\},$$

where $\Delta\theta_2$ is small. Then, the double Poincaré map $\mathscr{P}^{\theta_{20}, \Delta\theta_2} : \Sigma^{\theta_{20}, \Delta\theta_2} \rightarrow \Sigma^{\theta_{20}, \Delta\theta_2}$ is well defined. Furthermore, we compute the spectrum of Lyapunov exponents for each case by the method for impact sys-
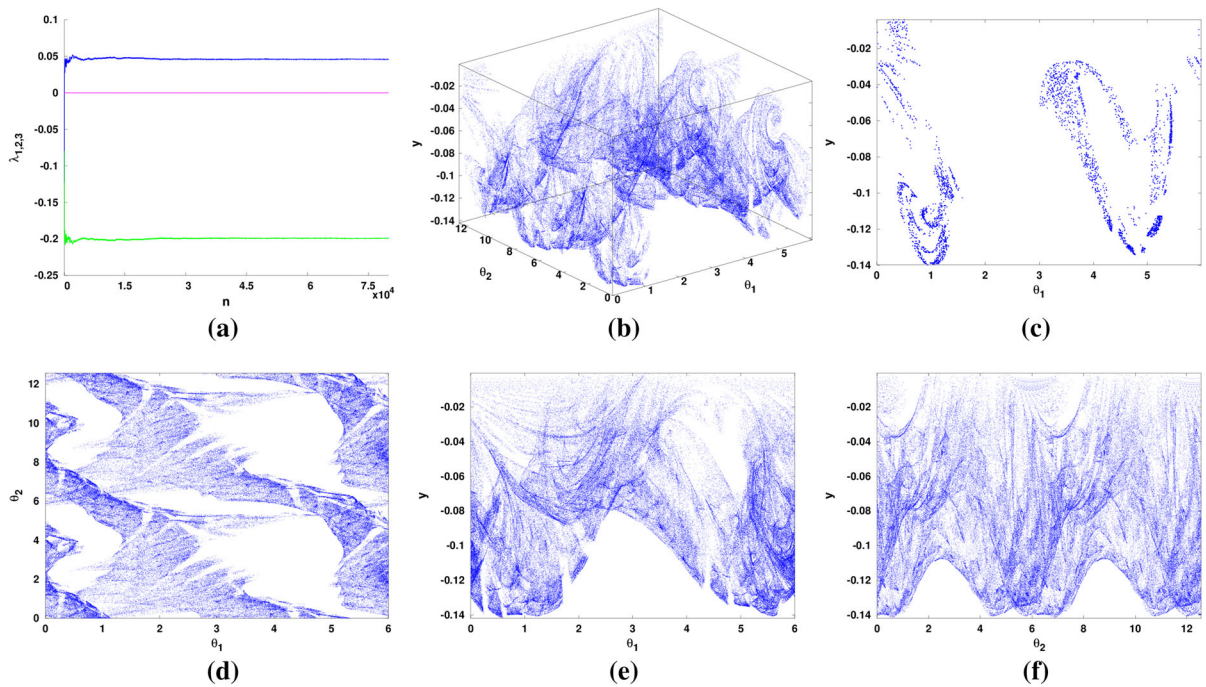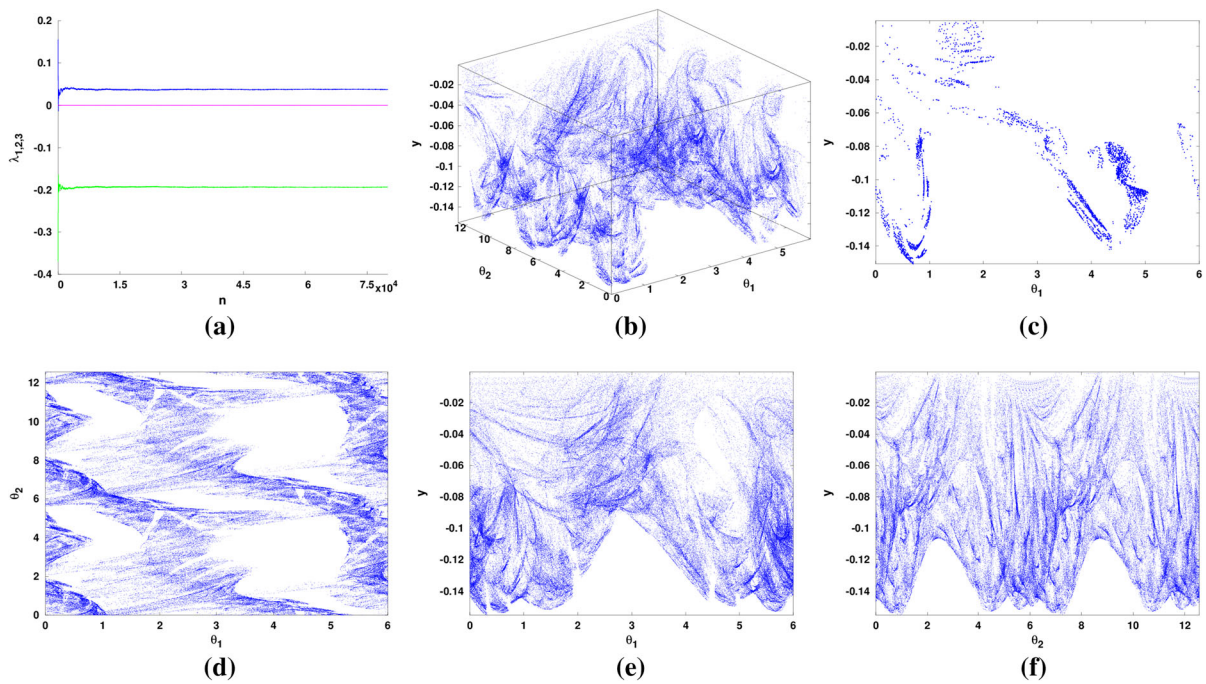
Fig. 7 Parameters are chosen from $\mathscr{C}_2$ with $\gamma_1 = \gamma_m$, $\gamma_2 = 1$, $\omega_2 = 0.5$, $\bar{\theta}_{10} = 0.5\pi$ and $\bar{\theta}_{20} = 1.6$. **a** Convergent sequences of the Lyapunov exponents, **b** the Poincaré map, **c** a projection of the double Poincaré map on to the (θ_1, y) plane, **d** a projection of the Poincaré map on to the (θ_1, θ_2) plane and **e** on to the (θ_1, y) plane and **f** on to the (θ_2, y) plane.

Fig. 8 Parameters are chosen from $\mathscr{C}_4$ with $\gamma_1 = \gamma_2 = \gamma_m$, $\omega_2 = 0.5$, $\bar{\theta}_{10} = \frac{\pi}{7}$ and $\bar{\theta}_{20} = 1$. **a** Convergent sequences of the Lyapunov exponents, **b** the Poincaré map, **c** a projection of the double Poincaré map on to the (θ_1, y) plane, **d** a projection of the Poincaré map on to the (θ_1, θ_2) plane and **e** on to the (θ_1, y) plane and **f** on to the (θ_2, y) plane.
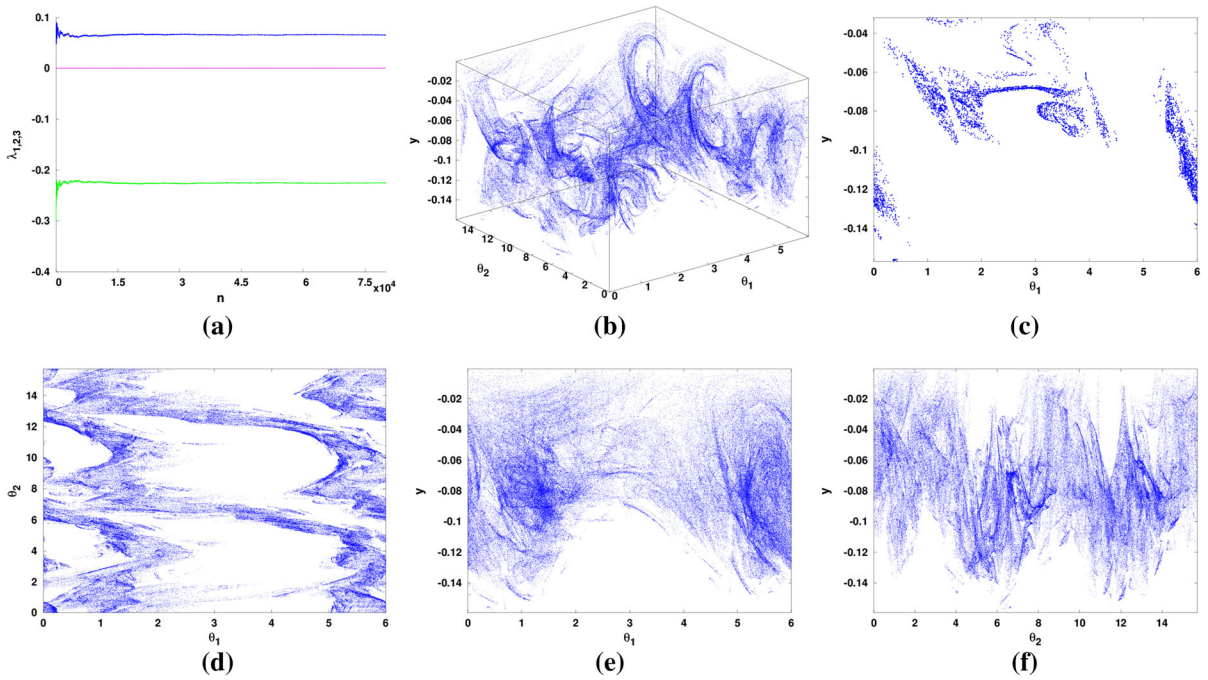
Fig. 9 Parameters are chosen from $\mathscr{C}_5$ with $\gamma_1 = 1.5$, $\gamma_2 = 1$, $\omega_2 = 0.4$ and $\bar{\theta}_{10} = \bar{\theta}_{20} = 0.5\pi$. **a** Convergent sequences of the Lyapunov exponents, **b** the Poincaré map, **c** a projection of the double Poincaré map on to the (θ_1, y) plane, **d** a projection of the Poincaré map on to the (θ_1, θ_2) plane and **e** on to the (θ_1, y) plane and **f** on to the (θ_2, y) plane.
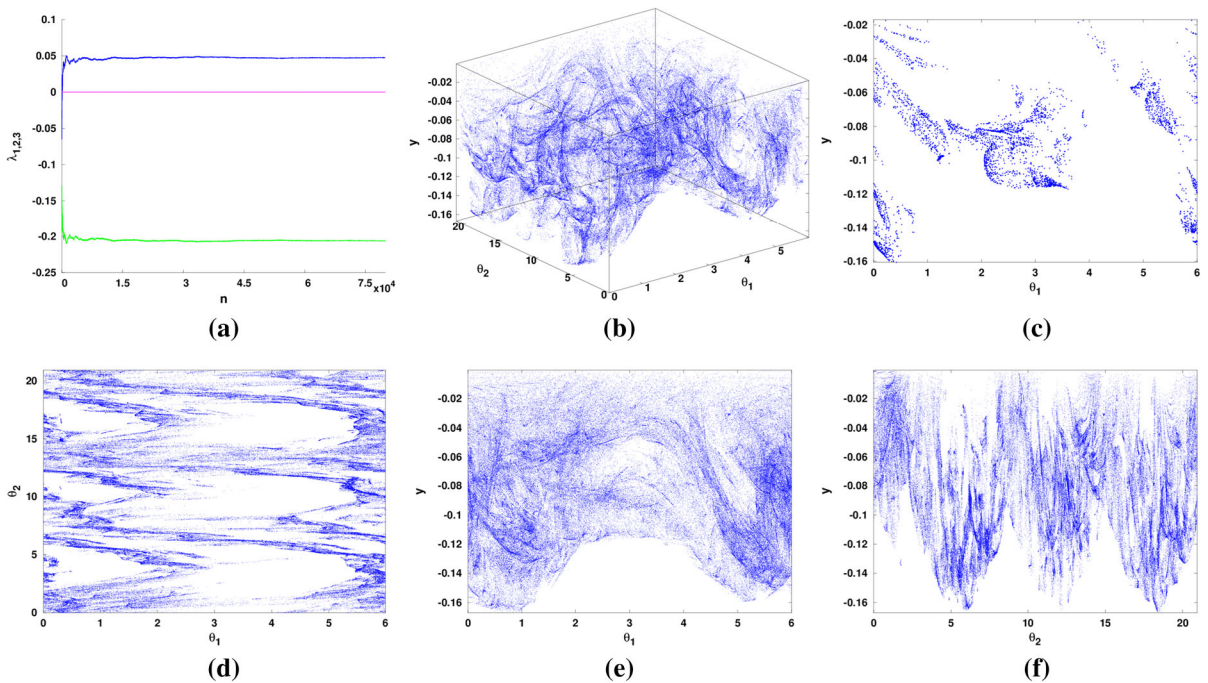

Fig. 10 Parameters are chosen from $\mathscr{C}_7$ with $\gamma_1 = 1.5$, $\gamma_2 = \gamma_m$, $\omega_2 = 0.3$, $\bar{\theta}_{10} = 0.4\pi$ and $\bar{\theta}_{20} = 1.55$. **a** Convergent sequences of the Lyapunov exponents, **b** the Poincaré map, **c** a projection of the double Poincaré map on to the (θ_1, y) plane, **d** a projection of the Poincaré map on to the (θ_1, θ_2) plane and **e** on to the (θ_1, y) plane and **f** on to the (θ_2, y) plane.
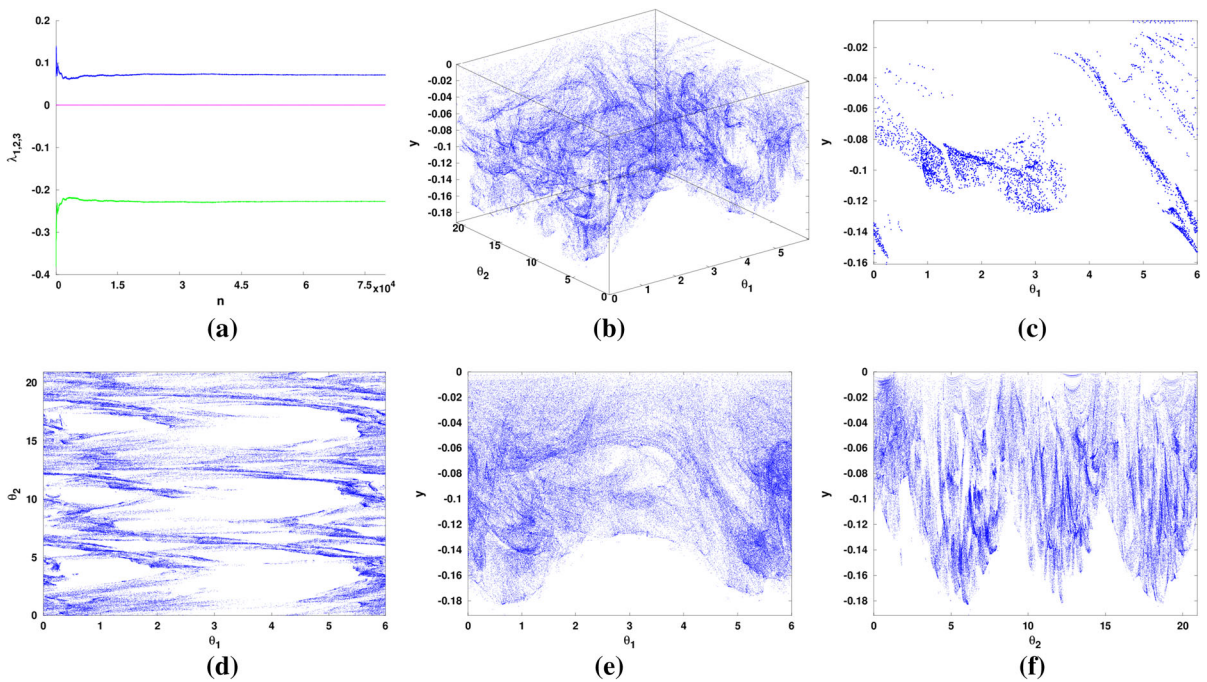
Fig. 11 Parameters are chosen from $\mathscr{C}_9$ with $\gamma_1 = 1.6$, $\gamma_2 = 1.5$, $\omega_2 = 0.3$, $\bar{\theta}_{10} = \frac{\pi}{3}$ and $\bar{\theta}_{20} = 1.5$. **a** Convergent sequences of the Lyapunov exponents, **b** the Poincaré map, **c** a projection of the double Poincaré map on to the (θ_1, y) plane, **d** a projection of the Poincaré map on to the (θ_1, θ_2) plane and **e** on to the (θ_1, y) plane and **f** on to the (θ_2, y) plane.

tems presented in [50,51] to verify the chaotic motions for the chosen parameters. It is elementary to prove that one of the three Lyapunov exponents is zero. Thus, we only need to compute the other two Lyapunov exponents. To approximate the Poincaré map $\mathscr{P} : \Sigma \mapsto \Sigma$, the fourth-fifth-order Runge–Kutta–Fehlberg method is chosen to solve system (13) for $|x| < 1$.

Since the left side of (17) is a linear combination of ρ and δ with constant coefficients, without the loss of generality, we fix $\rho = 0$ in this section. We also fix $\varepsilon = 0.04$, $\delta = 1.6$ and $\omega_1 = \frac{\pi}{3}$. Hence, $\alpha = \frac{\rho}{\sqrt{2}} + \frac{2\delta}{3}(2\sqrt{2} - 1) \approx 1.950322266$. Let $\gamma_m = \frac{\alpha}{4I_m} \approx 1.293904566$. Parameters γ_1, γ_2, and ω_2 are chosen from the chaotic zone for each case, so that system (13) exhibits chaotic behavior. In each case, we choose the values of $\bar{\theta}_{10}, \bar{\theta}_{20}$ and simulate an orbit of (13) starting from $(x_0 + 10^{-10}, y_0 + 10^{-10}, \bar{\theta}_{10}, \bar{\theta}_{20})$, where $y_0 = 0$, x_0 is the solution of the equation

$$x_0 - x_0^3 - \varepsilon \left(\gamma_1 \cos \bar{\theta}_{10} + \gamma_2 \cos \bar{\theta}_{20} \right) = 0. \quad (19)$$

Equation (19) is solved by the Newton–Raphson method with initial guess $x_0^0 = 0$. The Poincaré map $\mathscr{P} : \Sigma \mapsto \Sigma$ is iterated for 180,000 times with the first 2,000 iterations omitted for transients to decay. In each case, we plot (a) the convergent sequences in the iteration process of the spectrum of Lyapunov exponents; (b) the three-dimensional Poincaré map $\mathscr{P} : \Sigma \mapsto \Sigma$; (c) a projection of the double Poincaré map $\mathscr{P}^{\theta_{20}, \Delta\theta_2} : \Sigma^{\theta_{20}, \Delta\theta_2} \to \Sigma^{\theta_{20}, \Delta\theta_2}$ on to the (θ_1, y) plane; (d) a projection of the Poincaré map $\mathscr{P} : \Sigma \mapsto \Sigma$ on to the (θ_1, θ_2) plane and (e) on to the (θ_1, y) plane and (f) on to the (θ_2, y) plane.

In Table 1, the parameters chosen from the six chaotic zones $\mathscr{C}_k$ ($k = 1, 2, 4, 5, 7, 9$) for numerical simulations and the largest Lyapunov exponent $\lambda_{\max}$ are listed, where $\bar{\theta}_{10}$ and $\bar{\theta}_{20}$ are used to solve (19) to obtain initial conditions, θ_{20} and $\Delta\theta_2$ are used to define the double Poincaré map $\mathscr{P}^{\theta_{20}, \Delta\theta_2} : \Sigma^{\theta_{20}, \Delta\theta_2} \to \Sigma^{\theta_{20}, \Delta\theta_2}$. The results are shown in Figs. 6, 7, 8, 9, 10, and 11. From Table 1 and the figures, it is easy to see that for the chosen parameters for each chaotic zone, the largest Lyapunov exponent is positive and the double

Poincaré map has an attractor of fractal-like structure, suggesting that the system is chaotic. Therefore, the numerical experiments confirm our theoretical predictions.

5 Discussion and remarks

In this paper, we discussed for the first time the homoclinic bifurcation of a quasiperiodically excited nonlinear impact inverted pendulum. By using a method of Melnikov type, we extended the results of Ide and Wiggins [17,31,32] for homoclinic bifurcation of quasiperiodically excited smooth systems to the non-smooth ones. We are able to give a criterion for the appearance of Smale horseshoe-type chaotic dynamics of the system.

As an important application, by using a combination of analytical and numerical methods, we studied a quasiperiodically excited impact oscillator of Duffing type with two frequencies in detail. We give a complete description of the bifurcation sets and the chaotic zones in the parameter space. Numerical simulations have been performed for parameters chosen from the chaotic zones. The numerical results confirm the theoretical predictions.

It is worth mentioning that in addition to the work of Ide and Wiggins in [32], Parthasarathy also studied homoclinic bifurcation sets of quasiperiodically excited Duffing oscillator with two frequencies in [52]. Compared to their works, the main difference here is that the example considered in Sects. 3 and 4 is an impact system, which is non-smooth, while the systems studied in [32,52] are smooth. Hence, the expressions for the corresponding Melnikov functions are quite different. As can be seen from (16) that the Melnikov function $M_1(\theta_{10}, \theta_{20})$ computed in this paper involves in an additional parameter ρ due to the impact law given in (15), the integral $I(\omega)$ cannot be found analytically. Consequently, the resulting bifurcation sets for system (13) are different from those presented in [32,52]. Furthermore, the new feature of our work includes a comprehensive numerical simulations to validate the theoretical results, which is not a trivial task for non-smooth systems.

References

1. Awrejcewicz, J., Holicke, M.M.: Smooth and Nonsmooth High Dimensional Chaos and the Melnikov-Type Methods. World Scientific, Singapore (2007)
2. Bernardo, M.D., Budd, C.J., Champneys, A.R., Kowalczyk, P.: Piecewise-Smooth Dynamical Systems: Theory and Applications. Springer, London (2008)
3. Fečkan, M.: Topological Degree Approach to Bifurcation Problems. Springer, Dordrecht (2008)
4. Fečkan, M.: Bifurcation and Chaos in Discontinuous and Continuous Systems. Higher Education Press, Beijing (2011)
5. Ibrahim, R.A.: Vibro-Impact Dynamics: Modelling. Mapping and Applications. Springer, Berlin (2009)
6. Kunze, M.: Non-Smooth Dynamical Systems. Springer, Berlin (2000)
7. Colombo, A., Bernardo, M.D., Hogan, S.J., Jeffrey, M.R.: Bifurcations of piecewise smooth flows: perspectives, methodologies and open problems. Phys. D **241**, 1845–1860 (2012)
8. Makarenkov, O., Lamb, J.S.W.: Dynamics and bifurcations of nonsmooth systems: a survey. Phys. D **241**, 1826–1844 (2012)
9. Simpson, D.J.W., Meiss, J.D.: Aspects of bifurcation theory for piecewise-smooth, continuous systems. Phys. D **241**, 1861–1868 (2012)
10. Leine, R.I., van Campen, D.H., van de Vrande, B.L.: Bifurcations in nonlinear discontinuous systems. Nonlinear Dyn. **23**, 105–164 (2000)
11. Leine, R.I.: Bifurcations of equilibria in non-smooth continuous systems. Phys. D **223**, 121–137 (2006)
12. Casini, P., Vestroni, F.: Nonstandard bifurcations in oscillators with multiple discontinuity boundaries. Nonlinear Dyn. **35**, 41–59 (2004)
13. Battelli, F., Lazzari, C.: Exponential dichotomies, heteroclinic orbits, and Melnikov functions. J. Differ. Equ. **86**, 342–366 (1990)
14. Gruendler, J.: Homoclinic solutions for autonomous ordinary differential equations with nonautonomous perturbations. J. Differ. Equ. **122**, 1–26 (1995)
15. Guckenheimer, J., Holmes, P.: Nonlinear Oscillations. Dynamical Systems and Bifurcations of Vector Fields. Springer, New York (1983)
16. Melnikov, V.K.: On the stability of the center for time periodic perturbations. Trans. Mosc. Math. Soc. **12**, 1–57 (1963)
17. Wiggins, S.: Global Bifurcations and Chaos-Analytical Methods. Springer, New York (1988)
18. Yagasaki, K.: Detection of homoclinic bifurcations in resonance zones of forced oscillators. Nonlinear Dyn. **28**, 285–307 (2002)
19. Siewe, M.S., Yamgoué, S.B., Kakmeni, F.M.M., Tchawoua, C.: Chaos controlling self-sustained electromechanical seismograph system based on the Melnikov theory. Nonlinear Dyn. **62**, 379–389 (2010)
20. Battelli, F., Fečkan, M.: Homoclinic trajectories in discontinuous systems. J. Dyn. Differ. Equ. **20**, 337–376 (2008)
21. Battelli, F., Fečkan, M.: Chaos in forced impact systems. Discrete Contin. Dyn. Syst. Ser. S **6**, 861–890 (2013)

22. Carmona, V., Fernandez-Garcia, S., Freire, E., Torres, F.: Melnikov theory for a class of planar hybrid systems. Phys. D **248**, 44–54 (2013)

23. Du, Z., Zhang, W.: Melnikov method for homoclinic bifurcation in nonlinear impact oscillators. Comput. Math. Appl. **50**, 445–458 (2005)

24. Granados, A., Hogan, S.J., Seara, T.M.: The Melnikov method and subharmonic orbits in a piecewise-smooth system. SIAM J. Appl. Dyn. Syst. **11**, 801–830 (2012)

25. Kukučka, P.: Melnikov method for discontinuous planar systems. Nonlinear Anal. Ser. A **66**, 2698–2719 (2007)

26. Awrejcewicz, J., Fečkan, M., Olejnik, P.: Bifurcations of planar sliding homoclinics. Math. Prob. Eng. **2006**, 1–13 (2006)

27. Battelli, F., Fečkan, M.: Bifurcation and chaos near sliding homoclinics. J. Differ. Equ. **248**, 2227–2262 (2010)

28. Battelli, F., Fečkan, M.: An example of chaotic behaviour in presence of a sliding homoclinic orbit. Ann. Mat. Pura Appl. **189**, 615–642 (2010)

29. Battelli, F., Fečkan, M.: Nonsmooth homoclinic orbits, Melnikov functions and chaos in discontinuous systems. Phys. D **241**, 1962–1975 (2012)

30. Du, Z., Li, Y., Shen, J., Zhang, W.: Impact oscillators with homoclinic orbit tangent to the wall. Phys. D **245**, 19–33 (2013)

31. Wiggins, S.: Chaos in the quasiperiodically forced Duffing oscillator. Phys. Lett. A **124**, 138–142 (1987)

32. Ide, K., Wiggins, S.: The bifurcation to homoclinic tori in the quasiperiodically forced Duffing oscillator. Phys. D **34**, 169–182 (1989)

33. Moon, F.C., Holmes, W.T.: Double Poincaré sections of a quasi-periodically forced, chaotic attractor. Phys. Lett. A **111**, 157–160 (1985)

34. Vavriv, D.M., Ryabov, V.B., Sharapov, S.A., Ito, H.M.: Chaotic states of weakly and strongly nonlinear oscillators with quasiperiodic excitation. Phys. Rev. E **53**, 103–113 (1996)

35. Yagasaki, K.: Bifurcations and chaos in a quasi-periodically forced beam: theory, simulation and experiment. J. Sound Vib. **183**, 1–31 (1995)

36. Avramov, K.V., Awrejcewicz, J.: Frictional oscillations under the action of almost periodic excitation. Meccanica **41**, 119–142 (2006)

37. Chow, S.-N., Shaw, S.W.: Bifurcations of subharmonics. J. Differ. Equ. **65**, 304–320 (1986)

38. Shaw, S.W., Rand, R.H.: The transition to chaos in a simple mechanical system. Int. J. Non-linear Mech. **24**, 41–56 (1989)

39. Shaw, S.W., Haddow, A.G., Hsieh, S.-R.: Properties of cross-well chaos in an impacting system. Philos. Trans. R. Soc. Lond. A **347**, 391–410 (1994)

40. Lenci, S.: On the suppressions of chaos by means of bounded excitations in an inverted pendulum. SIAM J. Appl. Math. **58**, 1116–1127 (1998)

41. Lenci, S., Rega, G.: A procedure for reducing the chaotic response region in an impact mechanical system. Nonlinear Dyn. **15**, 391–409 (1998)

42. Lenci, S., Rega, G.: Periodic solutions and bifurcations in an impact inverted pendulum under impulsive excitation. Chaos Solitons Fractals **11**, 2453–2472 (2000)

43. Lenci, S., Rega, G.: Regular nonlinear dynamics and bifurcations of an impacting system under general periodic excitation. Nonlinear Dyn. **34**, 249–268 (2003)

44. Demeio, L., Lenci, S.: Asymptotic analysis of chattering oscillations for an impacting inverted pendulum. Q. J. Mech. Appl. Math. **59**, 419–434 (2006)

45. Du, Z., Li, Y., Zhang, W.: Type I periodic motions for nonlinear impact oscillators. Nonlinear Anal. Ser. A **67**, 1344–1358 (2007)

46. Li, Y., Du, Z., Zhang, W.: Asymmetric type II periodic motions for nonlinear impact oscillators. Nonlinear Anal. Ser. A **68**, 2681–2696 (2008)

47. Shen, J., Du, Z.: Double impact periodic orbits for an inverted pendulum. Int. J. Non-linear Mech. **46**, 1177–1190 (2011)

48. Piiroinen, P.T., Kuznetsov, Y.A.: An event-driven method to simulate Filippov systems with accurate computing of sliding motions. ACM Trans. Math. Softw. 34(3), Article no. 13 (2008).

49. Mancho, A.M., Small, D., Wiggins, S., Ide, K.: Computation of stable and unstable manifolds of hyperbolic trajectories in two-dimensional, aperiodically time-dependent vector fields. Phys. D **182**, 188–222 (2003)

50. Jin, L., Lu, Q.-S., Twizell, E.H.: A method for calculating the spectrum of Lyapunov exponents by local maps in non-smooth impact-vibrating systems. J. Sound Vib. **298**, 1019–1033 (2006)

51. Yue, Y., Xie, J., Gao, X.: Determining Lyapunov spectrum and Lyapunov dimension based on the Poincaré map in a vibro-impact system. Nonlinear Dyn. **69**, 743–753 (2012)

52. Parthasarathy, S.: Homoclinic bifurcation sets of the parametrically driven Duffing oscillator. Phys. Rev. A **46**, 2147–2150 (1992)